1996ApJ...463...95T

THE ASTROPHYSICAL JOURNAL, 463:95–104, 1996 May 20
© 1996. The American Astronomical Society. All rights reserved. Printed in U.S.A.

PINPOINTING THE CENTER OF ACTIVITY IN COMPACT SYMMETRIC OBJECTS. I. SOURCES FROM THE PEARSON-READHEAD SURVEY

G. B. TAYLOR,[1] A. C. S. READHEAD, AND T. J. PEARSON
California Institute of Technology, Pasadena, CA 91125; gtaylor@nrao.edu
Received 1995 August 31; accepted 1995 December 15

ABSTRACT

We use multifrequency, multiepoch VLBA observations to pinpoint the center of activity (or "core") in five compact symmetric objects (CSOs) and one candidate CSO from the Pearson-Readhead sample. We provide a first identification of the core component in two sources, and we have discovered that the cores of the objects 0108+388 and 2352+495 were previously misidentified. The precise location of the central engine in CSOs is crucially important for understanding their interaction with the surrounding environment and their evolution. All six objects studied here are found to display considerable asymmetry in their jets, especially near the core. The likely cause of this asymmetry is differences in density of the surrounding medium.

Subject headings: galaxies: compact — galaxies: jets — galaxies: nuclei — intergalactic medium — radio continuum: galaxies

1. INTRODUCTION

One of the most interesting findings from the flux limited VLBI survey of Pearson & Readhead (1988, hereafter PR) and from the complementary First Caltech–Jodrell Bank survey (hereafter CJ1 [Polatidis et al. 1995; Thakkar et al. 1995; Xu et al. 1995]) and Second Caltech–Jodrell Bank survey (hereafter CJ2 [Taylor et al. 1994; Henstock et al. 1995]) has been the discovery of six compact symmetric objects (CSOs) and 28 additional candidate CSOs in the nuclei of galaxies and quasars. These are compact (overall size <1 kpc) sources with lobe emission on both sides of the central engine that is thought to be relatively free of beaming effects (Wilkinson et al. 1994). Readhead et al. (1996b) found that these objects are almost certainly small because they are young (ages 10^3–10^4 yr) and not due to a dense confining medium. The advance speeds for the working surfaces, or "hot spots," in the CSOs was estimated to be $\sim 0.02c$. Readhead et al. (1996a) have proposed a unifying evolutionary model for powerful radio sources in which CSOs evolve first into compact steep spectrum doubles and then into large Fanaroff-Riley (1974) type II objects. Based on a different sample of objects, Fanti et al. (1995) reached the same conclusions. The precise location of the central engine is crucially important to the identification and understanding of this intriguing class of objects.

The only way to confirm the identification of a CSO candidate is by demonstrating two-sided ejection on scales smaller than 1 kpc. This usually requires the positive identification of the central engine, although one object has been identified as a CSO based on bidirectional motion in the central jet components (1946+708; Taylor, Vermeulen, & Pearson 1995). Given the low flux densities and strongly inverted spectra of most CSO cores (see § 3), progress in confirming and understanding CSOs has been slow. While Phillips & Mutel (1980, 1982) first drew attention over a decade ago to a class of "compact double" sources (CDs), which are almost certainly CSOs, definitive proof that the two components in these objects straddle the central engine has been elusive. Some CDs were even found to be asymmetric core-jet sources in which a compact jet component happened to appear similar to the core component at the discovery frequency (Conway et al. 1994). And in the CSOs 0108+388 (Conway et al. 1994) and 2352+495 (Conway et al. 1992), a strong compact jet component was tentatively identified as the core. Sensitive, multifrequency, multiepoch observations are therefore essential for correctly identifying the core component.

We present high-frequency, high-spatial resolution VLBA observations of six CSO and CSO candidate sources from the PR survey. Observations of the remaining CSO candidate from the PR survey, 2342+821, are reported on by Polatidis et al. (1995) and by Dallacasa et al. (1995). We use data obtained at multiple frequencies and multiple epochs and employ spectral criteria, component motions, and source morphologies to pinpoint the center of activity in each source.

2. OBSERVATIONS AND DATA REDUCTION

The observations were carried out at 8.4 and 15 GHz using the Very Long Baseline Array (VLBA)[2] telescope on 1994 December 21–22, 1995 March 22, and 1995 May 28. The details of the observations are provided in Table 1. Both right and left circular polarizations were recorded with 2 bit sampling. All sources were observed with 5–8 scans spread across a wide range in hour angle in order to obtain good u-v coverage. The VLBA correlator produced 64 frequency channels across every 8 MHz of observing bandwidth in each 4 s integration.

After correlation, global fringe fitting was performed using the AIPS task FRING, an implementation of the Schwab & Cotton (1983) algorithm. The fringe fitting was performed using a solution interval of 3.5 and 6.5 minutes for the 8 and 15 GHz data, respectively, with the least-squares option and the assumption of a point source model in all cases. Once delay and rate solutions had been applied the data were averaged in frequency to 8 MHz.

Amplitude calibration for each antenna was derived from

[1] Now at the National Radio Astronomy Observatory, Socorro, NM 87801.

[2] The National Radio Astronomy Observatory is operated by Associated Universities, Inc., under cooperative agreement with the National Science Foundation.

© American Astronomical Society • Provided by the NASA Astrophysics Data System

1996ApJ...463...95T

TABLE 1

OBSERVATIONAL PARAMETERS

Source	Date	Frequency (GHz)	Bandwidth (MHz)	Scan Length (minutes)	Total Time (hr)
0108+388.....	1994 Dec 21	15.4	8	26	2.2
0404+768.....	1995 May 28	8.4	16	6.5	0.5
0710+439.....	1994 Dec 21	15.4	16	13	1.3
1031+567.....	1995 Mar 22	8.4	16	6.5	0.5
	1995 May 28	15.4	16	13	1.4
1358+624.....	1994 Dec 21	8.4	16	6.5	0.8
2352+495.....	1994 Dec 21	15.4	8	26	3.5

measurements of the antenna gain and system temperature during each run. In addition, the strong calibrators 0300+470, 0552+398, and/or 1641+399 were observed in each run to further refine the amplitude calibration. After phase self-calibration with a 10 s solution interval and a point-source model, the data were coherently averaged to 30 s integrations. All editing, imaging, deconvolution, and self-calibration were performed using DIFMAP (Shepherd, Pearson, & Taylor 1994, 1995). Several iterations of phase self-calibration and imaging were performed upon each source before any attempt at amplitude self-calibration. At each iteration, windows for clean components were added, if necessary, to provide support and reject sidelobes. In all cases where we compare our data with data from previous epochs we have gone back to the calibrated *u-v* data and reimaged it in the fashion just described. It is important to note that spectral index maps made from two data sets with substantially different *u-v* coverages (such as we present here) may suffer from significant systematic errors, especially in regions of extended emission.

3. RESULTS

Below we present the results of our latest observations and any relevant comparison with previous observations for the purposes of identifying the center of activity. The identifications and redshifts are given for each target source in Table 2. The properties of the core components are summarized in Table 3. Throughout this paper we assume an Einstein–de Sitter universe with a Hubble constant $H_0 = 100\,h$ km s^{-1} Mpc^{-1}.

3.1. *0108+388*

The object 0108+388 was originally classified as a compact double in the PR survey. Subsequent observations by Conway et al. (1994) resolved both main components and revealed an additional central component at 10.7 GHz. In Figure 1*a* we show our uniformly weighted 15 GHz image. This image shows continuous emission connecting the two main components (labeled C1 through C7). This image also reveals an "S" symmetry which is a common feature in CSOs (Taylor et al. 1995; Readhead et al. 1995a). Conway et al. quote an upper limit of 0.18 $h^{-1}c$ on the separation velocity of the two main components (C1 and C7), based on 5 GHz observations at three epochs. By comparing our 15 GHz observations with the 1984 epoch 10.7 GHz observations of Conway et al. we find an increase in separation of 0.11 ± 0.1 mas in 10.9 yr, corresponding to an expansion velocity of 0.22 ± 0.20 $h^{-1}c$ between the two outer components. For component C5 we measure a significant motion with respect to both outer components. The motion of C5 with respect to the southwest component (C1) is 0.47 ± 0.1 mas, corresponding to a velocity of 0.92 ± 0.20 $h^{-1}c$ in the direction of the northeast component (C7). The model fits from which these velocities were derived are listed in Table 4. The error estimates on the motions derived above are only approximate since differences in observing frequency, and more importantly, in *u-v* coverage between the 10.7 and 15.4 GHz observations are substantial.

Observations at 8.4 GHz by Xu (1994) show "S" symmetry, although the emission from the central regions is weaker. In Figure 1*b* we show a spectral index map made from the 8.4 and 15 GHz images convolved to the same resolution. The spectral indices, defined $S_\nu \propto \nu^\alpha$, of the two outer components C1 and C7 are both − 0.7 ± 0.1, and the inner component C3 is strongly inverted with a spectral index of 3.0 ± 0.3. This value is somewhat steeper than the maximum spectral index of 2.5 for synchrotron self-absorption in the case of a single power-law distribution of electron energies, but other plausible electron energy distributions can produce a steeper spectrum (de Kool & Begelman 1989). Alternatively, since the observations were separated by 1.8 yr, it is possible that variability of C3 may have introduced a substantial error in our derived spectral index.

Based on their prominent location at each end of the source, low separation velocity, and steep spectral indices we identify components C1 and C7 as the working surfaces of two oppositely directed jets. Based on its strongly inverted spectrum and location near the center of symmetry of the source, we identify C3 with the center of activity. We note that while C5 also has an inverted spectrum ($\alpha = 0.2$), its large apparent motion toward the east lobe makes it more likely to be a strong, compact component in a relativistic jet.

TABLE 2

SOURCE IDENTIFICATIONS

Source (1)	R.A. (2)	Declination (3)	*V* (4)	ID (5)	*z* (6)
0108+388.....	01^{h}11^{m}37^s.3118	39°06′28″.110	22	G	0.699
0404+768.....	04 10 46.5599	76 56 45.155	22	G	0.5985
0710+439.....	07 13 38.1766	43 49 17.005	21	G	0.518
1031+567.....	10 35 07.0451	56 28 46.697	20	G	0.4597
1358+624.....	14 00 28.6503	62 10 38.508	21	G	0.431
2352+495.....	23 55 09.4539	49 50 08.362	20	G	0.2383

NOTES.—Col. (1): B1950 Source name according to IAU convention. Cols. (2)–(3): J2000.0 right ascension and declination (Patnaik et al. 1992). Col. (4): Visual magnitude (Pearson & Readhead 1988). Col. (5): Optical identification: G, galaxy. Col. (6): Redshift (Lawrence et al. 1996).

© American Astronomical Society • Provided by the NASA Astrophysics Data System

1996ApJ...463...95T

TABLE 3

CORE IDENTIFICATIONS AND PARAMETERS

Source (1)	Core Size (2)	Core Flux (3)	Total Flux (4)	Core Fraction (5)	Core Spectral Index (6)
0108+388	≤0.29	10 ± 2	480 ± 20	0.021	3.0 ± 0.3
0404+768[a]	≤0.50	140 ± 14	2320 ± 100	0.060	0.03 ± 0.3
0710+439	≤0.56	45 ± 5	760 ± 30	0.059	0.8 ± 0.3
1031+567	N/A	<2	450 ± 15	<0.004	N/A
1358+624[a]	≤0.30	17 ± 2	1250 ± 70	0.014	1.7 ± 0.4
2352+495	≤0.64	12 ± 3	630 ± 20	0.019	0.14 ± 0.3

NOTES.—Col. (1): Source name. Col. (2): Size of core in milliarcseconds. Col. (3): Flux density of core in mJy at 15 GHz. Col. (4): Total flux density at 15 GHz from preliminary observations by the University of Michigan Radio Observatory. Col. (5): Core fraction defined as the ratio of the core flux density to the total flux density at the observed frequency of 15 GHz unless otherwise noted. No attempt at k-correcting these values has been made. Col. (6): Spectral index of core at high radio frequency (≥5 GHz).

[a] Flux densities are measured at 8.4 GHz.

3.2. *0404+768*

The 1.7 GHz observations of 0404+768 by Polatidis et al. (1995) (Fig. 2*a*) and by Dallacasa et al. (1995) show two similar extended "lobes" and a bright, well-collimated jet on one side. Xu et al. (1995) reports a compact component at 5 GHz located at the base of the strongly jetted side. This component is roughly midway between the two radio lobes and has an inverted spectral index measured between 1.7 and 5 GHz of 0.52 (Xu 1994). Our 8.4 GHz image (Fig. 2*b*) shows this compact component to be more prominent and compact, with a spectral index between 5 and 8.4 GHz of +0.03. The more diffuse lobe emission on the northeast side has been completely lost due to a lack of short spacings. The total flux density recovered in our 8.4 GHz image is about half of the total flux density reported by the University of Michigan Radio Astronomy Observatory. Based on its spectrum and location we identify the strong compact component in our 8.4 GHz image with the center of activity. Dallacasa et al. (1995) tentatively identified the radio core with this same component. While there is high-luminosity emission on both sides of the core, no hot spots are readily identifiable in this object.

3.3. *0710+439*

This was the first compact source found with a triple structure (Readhead, Pearson, & Unwin 1984). Based on observations at 5 and 10 GHz, Readhead et al. found that the two outer components had a steep spectrum, while the inner components had a flat spectrum at the southernmost end. Observations at 1.7 and 5 GHz (Wilkinson et al. 1994) reveal weak, steep-spectrum lobes that give this source "S" symmetry as well. Conway et al. (1994) place a 3 σ upper limit on the relative motion between the northern and middle components (A and B) of 0.41 $h^{-1}c$ using three 5 GHz observations spread over a 6 yr interval. In Figure 3*a* we show our 15 GHz observations which resolve all three of the components reported by Readhead et al. (1984). Components A and C are both leading-edge brightened with emission fading gradually toward the center of the source. Component B is more compact at the southern end and becomes wider to the north with an opening angle of ~20°. In Figure 3*b* we show a spectral index map made from the 8.4 (Xu 1994) and 15 GHz images convolved to the same resolution. The extreme north and south components have spectral indices of −0.3 and −0.8, respectively. The inner

TABLE 4

GAUSSIAN MODEL AND PROPER MOTIONS FOR 0108+388

Component	Epoch	S (Jy)	r (mas)	θ	a (mas)	b/a	Φ	v (mas yr^{-1})	P.A.
C1	1994	0.118	2.50	−123°.8	0.53	0.74	−30°.5		
	1984	0.119	2.50	−123.8	0.50	0.46	−62.9	Reference	
C2	1994	0.034	1.85	−139.7	0.82	0.72	66.4		
	1984	0.029	2.04	−132.0	1.01	0.0	38.2	0.32 ± 0.3	98°
C3	1994	0.010	0.0	0.0	0.29	1.0	0.0		
	1984[a]								
C4	1994	0.038	1.17	51.5	0.89	0.20	74.7		
	1984[a]								
C5	1994	0.054	1.54	47.8	0.17	0.28	−76.6		
	1984	0.054	1.08	44.2	0.61	0.00	0.7	0.47 ± 0.1	56
C6	1994	0.104	2.36	59.0	0.93	0.37	−84.8		
	1984	0.149	2.43	57.6	0.94	0.00	89.7	0.09 ± 0.1	−163
C7	1994	0.172	3.34	62.4	0.47	0.48	−79.3		
	1984	0.247	3.27	61.1	0.60	0.0	−72.5	0.11 ± 0.1	109

NOTES.—Parameters of each Gaussian component of the model brightness distribution: S, flux density; r, θ, polar coordinates of the center of the component relative to an arbitrary origin, with polar angle measured from north through east; a, b, major and minor axes of the FWHM contour; Φ, position angle of the major axis measured from north through east; v, velocity of the component along the given position angle assuming that C1 is stationary.

[a] Not seen.

© American Astronomical Society • Provided by the NASA Astrophysics Data System

1996ApJ...463...95T

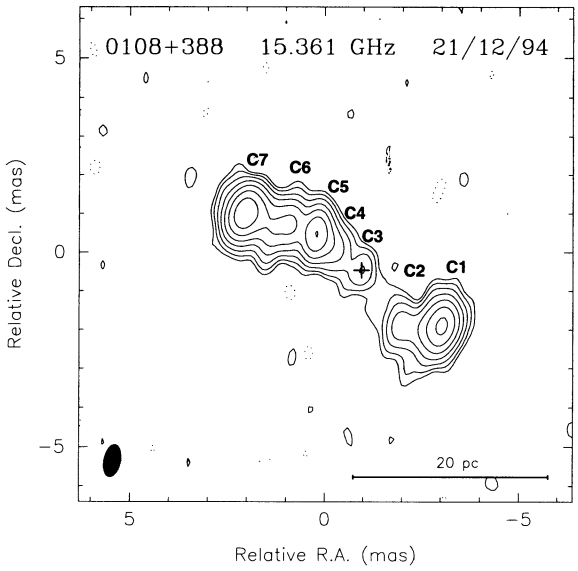

FIG. 1*a*

jet has a spectral index ranging from −0.4 at the northern end to 0.8 at the southern end (see inset to Fig. 3*b* below). Gaussian model fits are given in Table 5.

Based on their location at the source extremes, slow separation velocity, and steep spectral indices we identify components A and C as hot spots. Based on its strongly inverted spectrum and location near the center of symmetry of the source, we tentatively identify the compact southernmost subcomponent within B with the center of activity. These conclusions are identical to those reached by Readhead, Pearson, & Unwin (1984).

3.4. *1031+567*

This source was found to have a compact double morphology in unpublished 5 GHz observations by Pearson & Readhead. Here we present observations at 8.4 GHz (Fig. 4*a*) and 15.4 GHz (Fig. 4*b*). We have also made a spectral index map from uniformly weighted 5 GHz data and naturally weighted and suitably tapered 15 GHz data (Fig. 4*c*). This source is dominated by two leading edge-brightened components. The spectrum of both components is quite

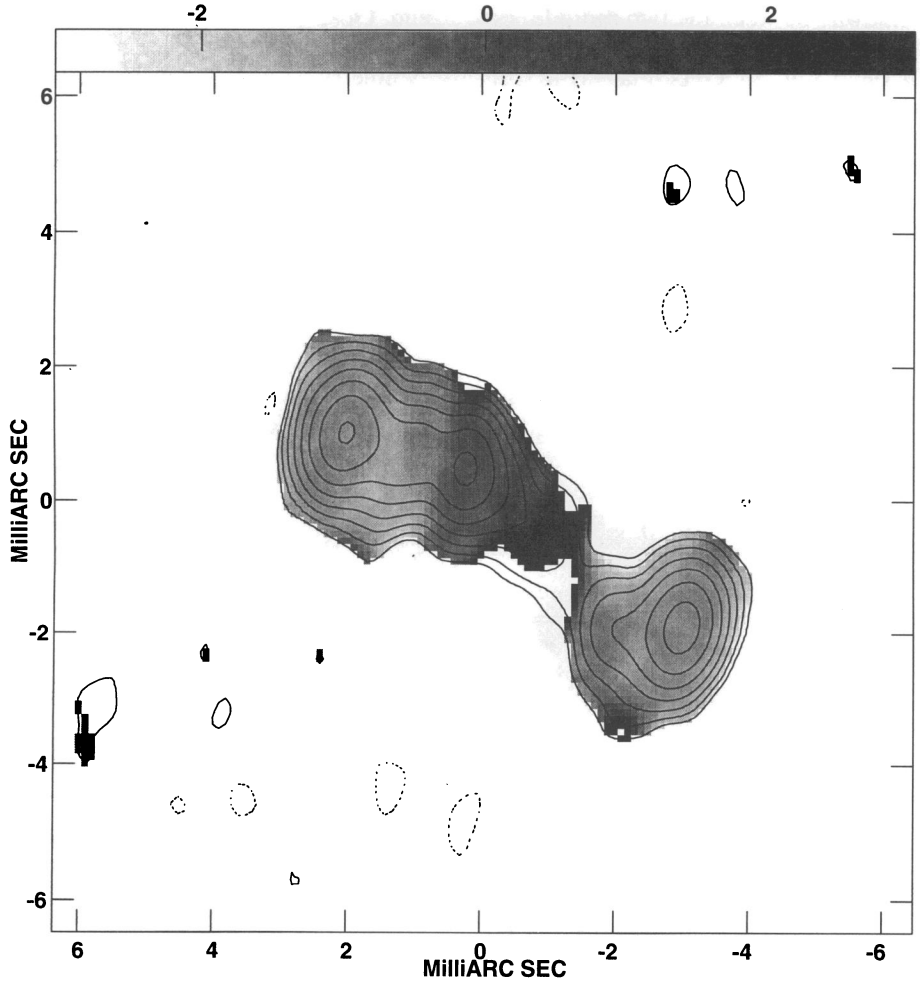

FIG. 1*b*

FIG. 1.—(*a*) The uniformly weighted 15 GHz VLBI image of 0108+388. Contours are drawn at −1, 1, 2, 4, ..., 64 mJy beam^{-1}. The cross marks the location of the center of activity as discussed in the text. The synthesized beam FWHM is drawn in the lower left-hand corner and has dimensions 0.83 × 0.42 mas in position angle −12°. (*b*) A spectral index map, defined $S_\nu \propto \nu^\alpha$ made by combining our 15 GHz observations with the 8.4 GHz observations by Xu (1994) at the same resolution of 1.05 × 0.58 mas in position angle −10°. The gray-scale range is from −3 to 3. Contours are overlaid from the naturally weighted 15 GHz VLBI image at −1, 1, 2, 4, ..., 128 mJy beam^{-1}.

© American Astronomical Society • Provided by the NASA Astrophysics Data System

1996ApJ...463...95T

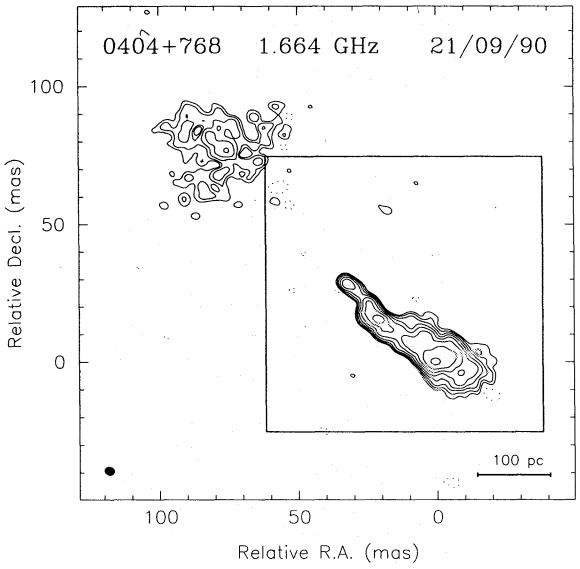

FIG. 2a

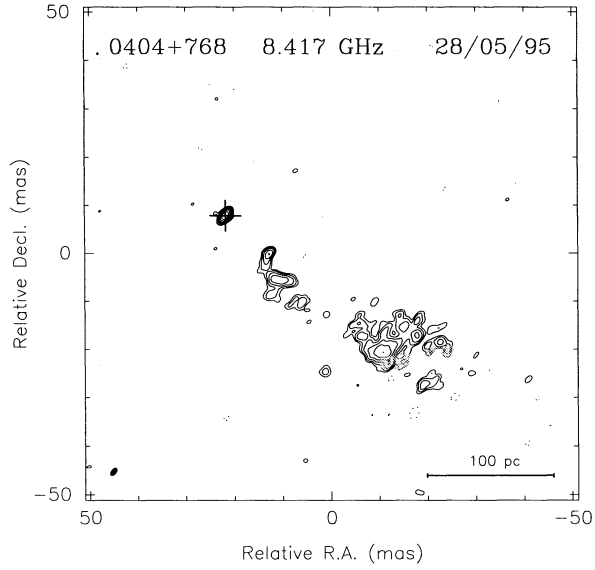

FIG. 2b

FIG. 2.—(*a*) The naturally weighted 1.7 GHz image of 0404+768 from Polatidis et al. (1995). Contours levels are drawn at −2, 2, 4, 8, ..., 256 mJy beam^{-1}. The synthesized beam FWHM is drawn in the lower left-hand corner and has dimensions 3.45 × 2.85 mas^2 in position angle 75°. The inset box marks the region shown in (*b*). (*b*) The naturally weighted 8.4 GHz VLBI image of 0404+768. Contours are drawn at −2, 2, 4, 8, ..., 64 mJy beam^{-1}. The cross marks the location of the center of activity as discussed in the text. The synthesized beam FWHM is drawn in the lower left-hand corner and has dimensions 1.81 × 0.99 mas in position angle −39°.

steep, with a spectral index between 5 and 15 GHz of -0.8 ± 0.1 and -1.1 ± 0.1 in the northeast and southwest components, respectively. At 8.4 GHz there is a weak (2.8 mJy), compact component to the southwest of the geometric center of the source. This component is also visible at 5 GHz and has a flux density of 7.9 mJy. This component is marginally detected in a tapered map at 15.4 GHz with a flux density of 1.7 mJy. Its spectral index between 5 and 8.4 GHz is -2 ± 1 and between 8.4 and 15 GHz is -0.9 ± 1. Variability of this component may have influenced the spectral index determined between 5 and 8.4 GHz since these observations are separated by 5 yr.

Given the edge-brightened appearance and steep spectra of the two outer components, it is likely that they are the working surfaces and lobes of two oppositely directed jets. It is therefore possible that the compact component near the center of the source coincides with the center of activity; however, the steep spectrum of this component at high frequencies is more typical of a jet component. Based on the available information we conclude that it is highly likely that 1031+567 is indeed a CSO, but we cannot yet pinpoint the center of activity.

TABLE 5

GAUSSIAN MODEL FOR 0710+439 AT 15 GHz

Component	S (Jy)	r (mas)	θ	a (mas)	b/a	Φ
A	0.134	11.50	−0°.0	0.48	0.27	69°.9
A	0.128	11.05	−0.5	1.15	0.43	89.8
	0.050	9.82	−1.8	3.59	0.35	−53.1
B	0.116	2.92	4.8	1.05	0.29	13.1
B	0.115	2.42	1.7	1.15	0.31	−25.5
B	0.122	1.28	0.4	0.46	0.25	15.8
B	0.045	0.0	0.0	0.56	0.33	−13.1
C	0.019	11.87	177.4	3.36	0.11	10.2
C	0.041	12.89	−177.3	1.08	0.58	−9.2

NOTES.—Parameters of each Gaussian component of the model brightness distribution: S, flux density; r, θ, polar coordinates of the center of the component relative to an arbitrary origin, with polar angle measured from north through east; a, b, major and minor axes of the FWHM contour; Φ, position angle of the major axis measured from north through east.

3.5. *1358+624*

This source is one of 11 low-frequency variable sources mapped using global VLBI observations by Padrielli et al. (1991) at 608 MHz. Padrielli et al. showed this source to be a double separated by 46 mas with a possible bridge of emission. Observations at 1.7 GHz by Dallacasa et al. (1995) confirm that the two lobes are connected by a knotty, broad jet. Unpublished observations by Pearson & Readhead at 5 GHz resolve the two lobes and a long, one-sided jet with a faint, compact component at the base. Our 8.4 GHz observations (Fig. 5*a*) show similar structure with a much stronger compact component at the base of the jet. The spectral index of this compact component between 5 and 8.4 GHz is 1.7 (see Fig. 5*b*). Based on its compactness, inverted spectral index, and location, we identify this component with the center of activity and confirm that 1358+624 is indeed a member of the CSO class. At 1.7 GHz 1358+624 appears more symmetrical than at higher frequencies (Dallacasa et al. 1995). There is no clear evidence for hot spots on either side of the central engine.

3.6. *2352+495*

The object 2352+495 was originally classified as a compact double in the first epoch of the PR survey. Conway et al. (1992), however, discovered a third component to the south, and 18 cm observations by Wilkinson et al. (1994) and Polatidis et al. (1995) revealed a symmetric structure and the presence of extended radio lobes. Other observations at centimeter, millimeter, optical, and X-ray wavelengths of this archetype CSO are discussed by Readhead et al. (1996b). The hot spots (labeled A and C after Conway et al. 1992) are well resolved in our 15 GHz image (Fig. 6*a*). A

© American Astronomical Society • Provided by the NASA Astrophysics Data System

1996ApJ...463...95T

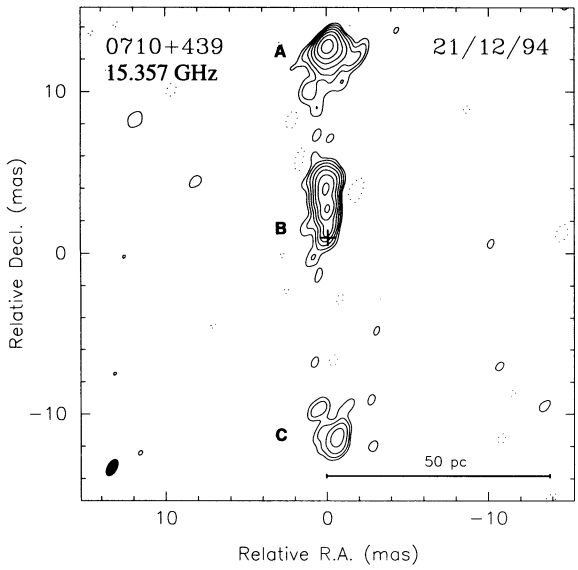

FIG. 3*a*

bright, complicated feature (B1 and B2) was suggested as the most likely location for the center of activity by Conway et al. based primarily on significant variability (>20%) over the 7 yr spread of their observations. Conway et al. also reported an apparent relative motion of component B1 toward component A of 0.42 $h^{-1}c$, which was difficult to understand if the center of activity was coincident with B1.

In our 15 GHz image we see a narrow jet to the south of component B1 with a compact component (D) embedded in it. The spectral index between 8 and 15 GHz of component D is 0.14, which is more inverted than any component in the B1-B2 complex (Fig. 6*b*). This component is very close to the midpoint defined by a line connecting the two hot spots A and C. We suggest that D is the core component, and that the B1-B2 complex is a bright inner jet moving relativistically toward hot spot A. The high surface brightness and large width of the B1-B2 complex may indicate that the jet has been disrupted in this region, perhaps due to an encounter with interstellar material. This identification of the central engine also leads to a more noticeable "S" symmetry in 2352+495, which appears to be a common feature

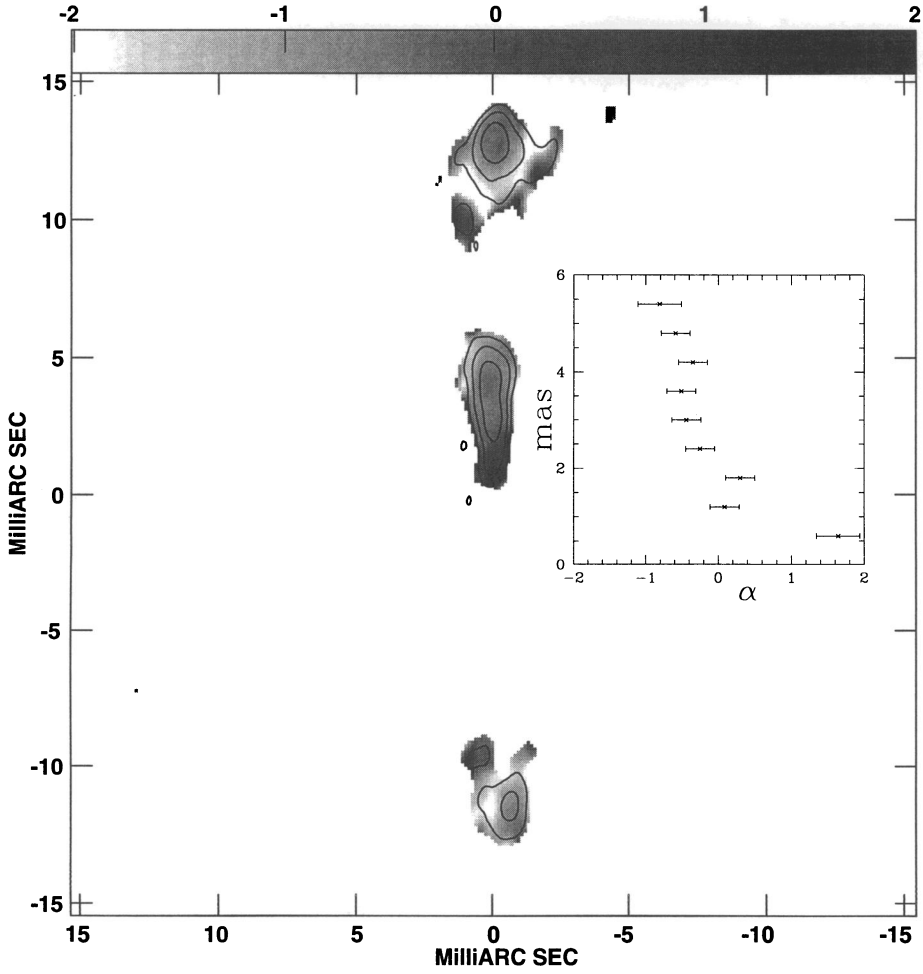

FIG. 3*b*

FIG. 3.—(*a*) The naturally weighted 15 GHz VLBI image of 0710+439. Contours are drawn at −1.5, 3, 6, 12, ..., 96 mJy beam^{-1}. The cross marks the location of the center of activity as discussed in the text. The synthesized beam FWHM is drawn in the lower left-hand corner and has dimensions 1.12 × 0.57 mas in position angle −29°. (*b*) A spectral index map made by combining our 15 GHz observations with the 8.4 GHz observations by Xu (1994) at the same resolution of 1.06 × 0.50 mas in position angle −10°. The gray-scale range is from −2 to 2. Contours are overlaid from the naturally weighted 15 GHz at −3, 3, 12, 48, and 192 mJy beam^{-1}. The inset graph shows the spectral index variation along the inner jet with distance from the map center.

© American Astronomical Society • Provided by the NASA Astrophysics Data System

1996ApJ...463...95T

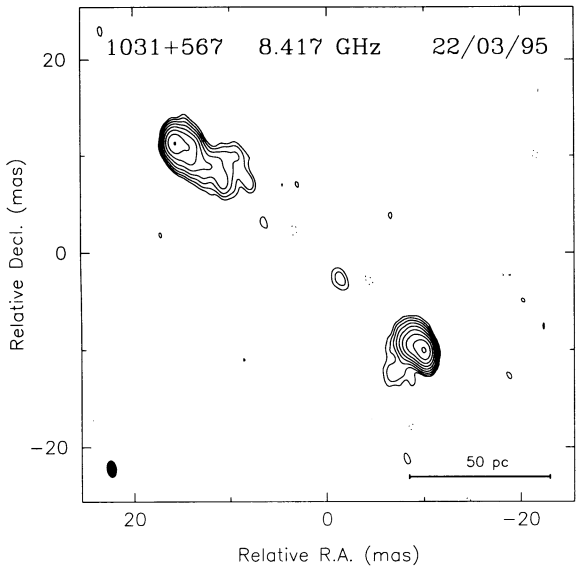

FIG. 4*a*

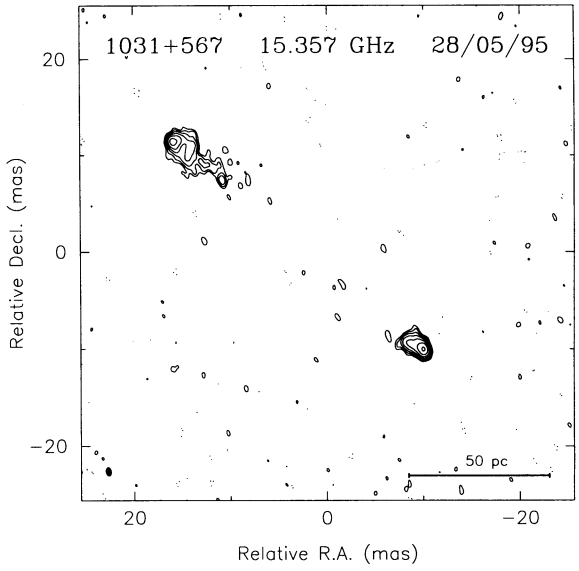

FIG. 4*b*

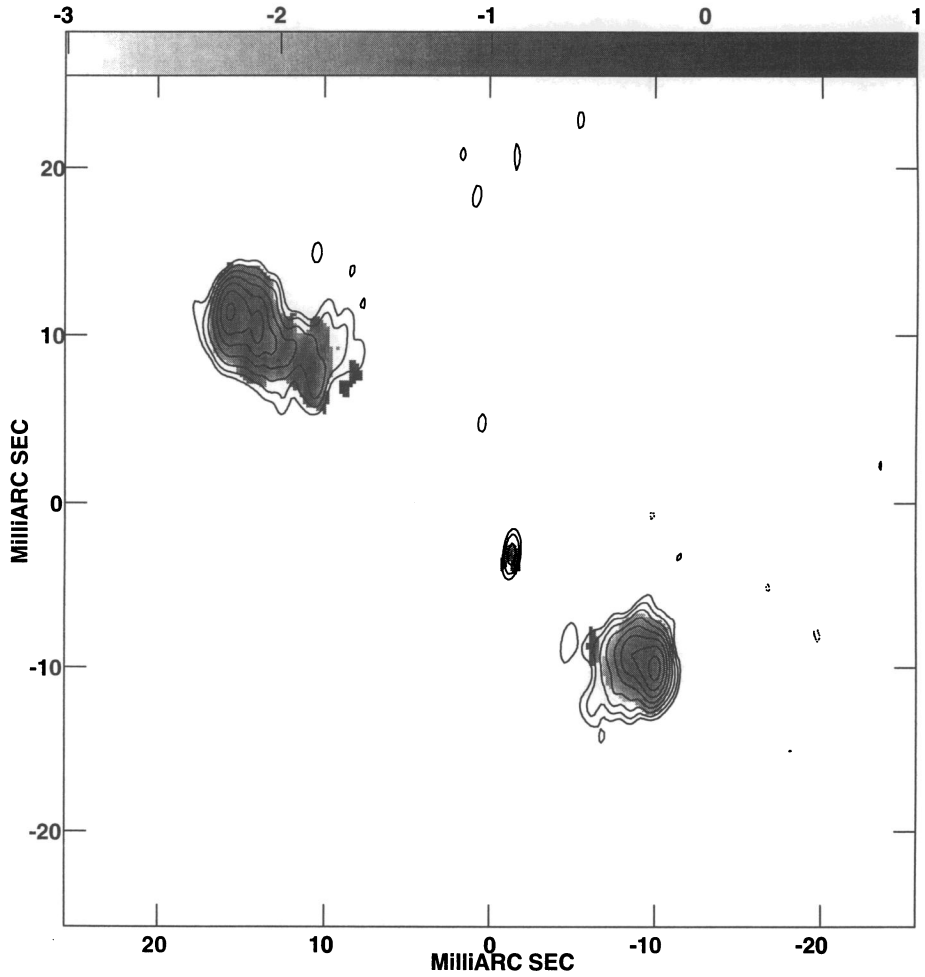

FIG. 4*c*

FIG. 4.—(*a*) The naturally weighted 8.4 GHz VLBI image of 1031+567. Contours are drawn at −0.75, 0.75, 1.5, 3, 6, ..., 192 mJy beam^{-1}. The synthesized beam FWHM is drawn in the lower left-hand corner and has dimensions 1.69 × 0.94 mas in position angle 8°. (*b*) The naturally weighted 15 GHz VLBI image of 1031+567. Contours are drawn at −0.75, 0.75, 1.5, 3, 6, ..., 48 mJy beam^{-1}. The synthesized beam FWHM is drawn in the lower left-hand corner and has dimensions 0.86 × 0.53 mas in position angle 10°. (*c*) A spectral index map made by combining our 15 GHz observations with unpublished 5 GHz observations by Pearson & Readhead at the same resolution of 2.10 × 0.72 mas in position angle −4°. The gray-scale range is from −3 to 1. Contours are overlaid from the uniformly weighted 5 GHz image with contour levels at −1.5, 1.5, 3, 6, ..., 192 mJy beam^{-1}.

© American Astronomical Society • Provided by the NASA Astrophysics Data System

1996ApJ...463...95T

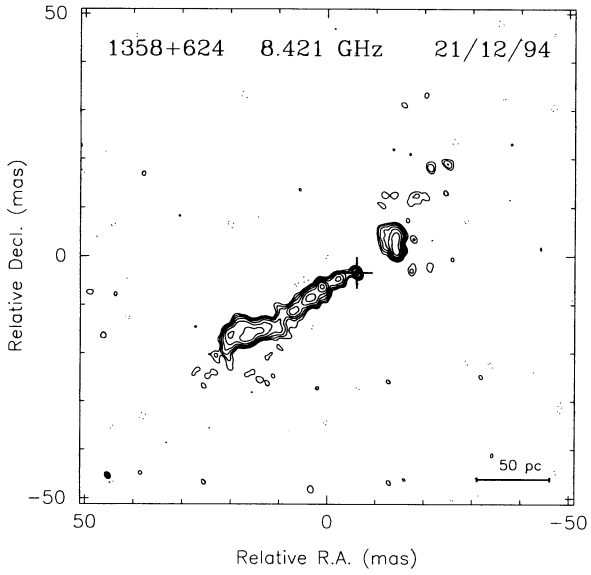

FIG. 5a

in CSOs. Estimates of the flux densities, locations, and sizes of the various components in 2352+495 at 15 GHz are given in Table 6. The spectral index between 8.4 and 15 GHz of the northern and southern hot spots is -0.38 ± 0.2 and -0.73 ± 0.4, respectively.

4. DISCUSSION

In Table 7 we present a score-card summary of our results for each of the six objects studied. Our identifications of the centers of activity show that there are substantial jet-to-counterjet brightness ratios (>10:1) in all five of the confirmed PR CSOs. So far only the one unconfirmed CSO (1031+567) lacks a strong, predominantly one-sided jet. Three possible interpretations for these large ratios are (1) relativistic beaming, (2) different external densities on the two sides, and (3) an intrinsic asymmetry in the jets. A problem with significant relativistic beaming is that the "core" components in the CSOs are generally quite weak (Table 3), making up typically less than 1% of the total source flux density at 5 GHz. If the jets are substantially Doppler boosted then it is reasonable to expect the core flux

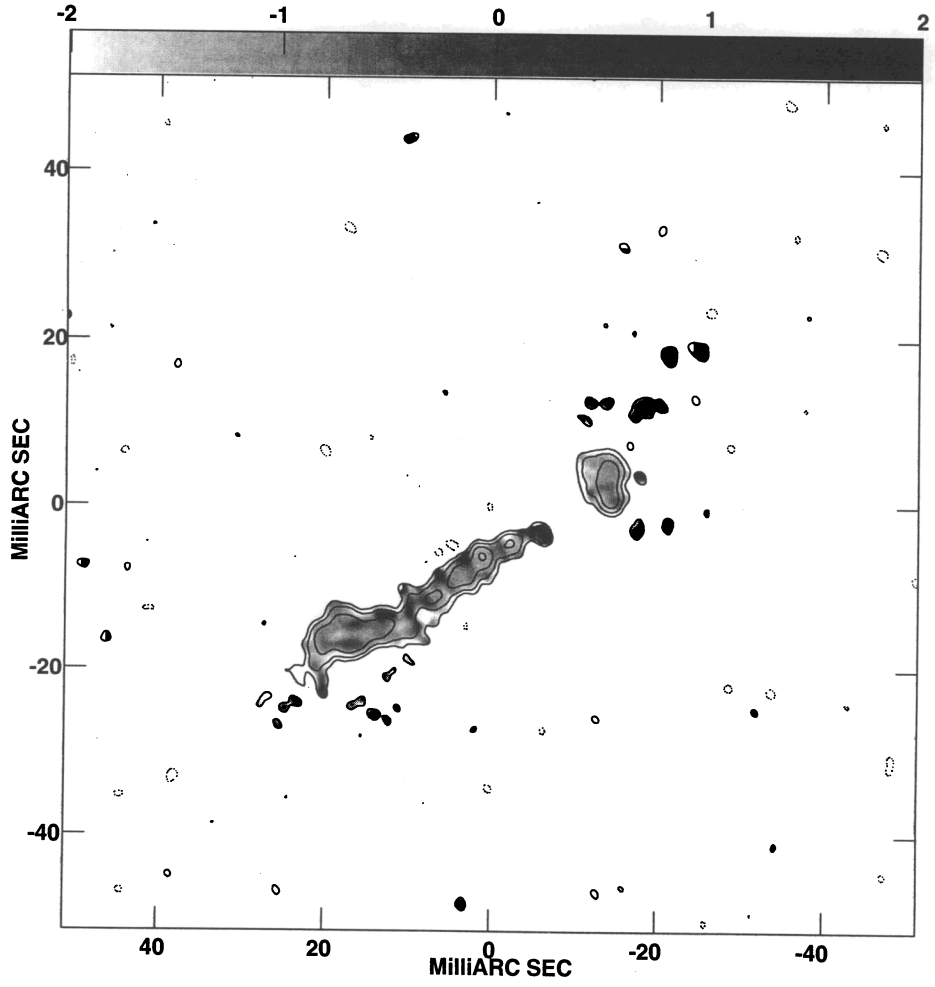

FIG. 5b

FIG. 5.—(*a*) The naturally weighted 8.4 GHz VLBI image of 1358+624. Contours are drawn at −0.75, 0.75, 1.5, 3, 6, ..., 48 mJy beam^{-1}. The synthesized beam is drawn in the lower left-hand corner and has dimensions 1.57 × 1.09 mas in position angle 34°. (*b*) A spectral index map made by combining our 8.4 GHz observations with unpublished 5 GHz observations by Pearson & Readhead at the same resolution of 1.57 × 1.09 mas in position angle 34°. The gray-scale range is from −2 to 2. Contours are overlaid from the naturally weighted 8.4 GHz image at −0.75, 0.75, 3, 12, and 48 mJy beam^{-1}.

© American Astronomical Society • Provided by the NASA Astrophysics Data System

1996ApJ...463...95T

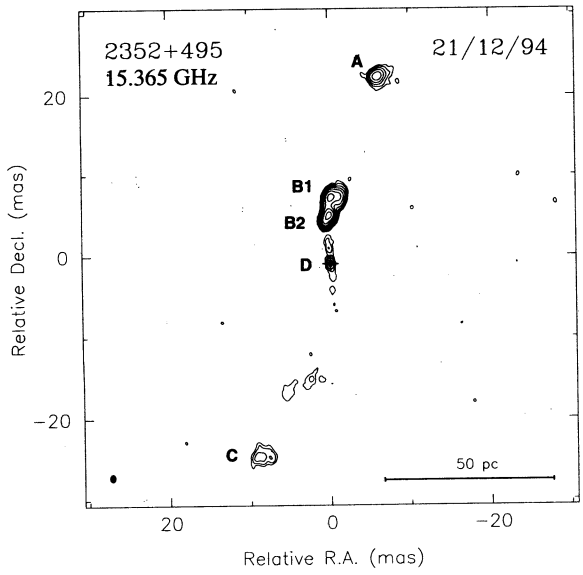

FIG. 6*a*

TABLE 6

GAUSSIAN MODELS FOR 2352+495 AT 15 GHz

Component	S (Jy)	r (mas)	θ	s (mas)	b/a	Φ
A	0.054	24.08	−14°.4	1.20	0.69	−68°.2
B1	0.085	8.31	−6.9	1.20	0.70	−5.8
B1	0.120	8.21	−0.0	0.94	0.63	−25.4
B2	0.073	6.60	2.4	1.56	0.39	0.4
B2	0.157	6.02	0.7	0.60	0.80	−54.3
B2	0.083	5.36	6.3	0.53	0.53	8.4
	0.007	2.18	5.2	1.69	0.20	5.3
D	0.012	0.00	0.0	0.64	0.17	4.1
	0.003	3.43	−175.6	0.77	0.51	−70.5
	0.022	15.07	167.2	6.45	0.27	−61.6
C	0.025	25.23	159.9	2.06	0.61	−81.0

NOTES.—Parameters of each Gaussian component of the model brightness distribution: S, flux density; r, θ, polar coordinates of the center of the component relative to an arbitrary origin, with polar angle measured from north through east; a, b, major and minor axes of the FWHM contour; Φ, position angle of the major axis measured from north through east.

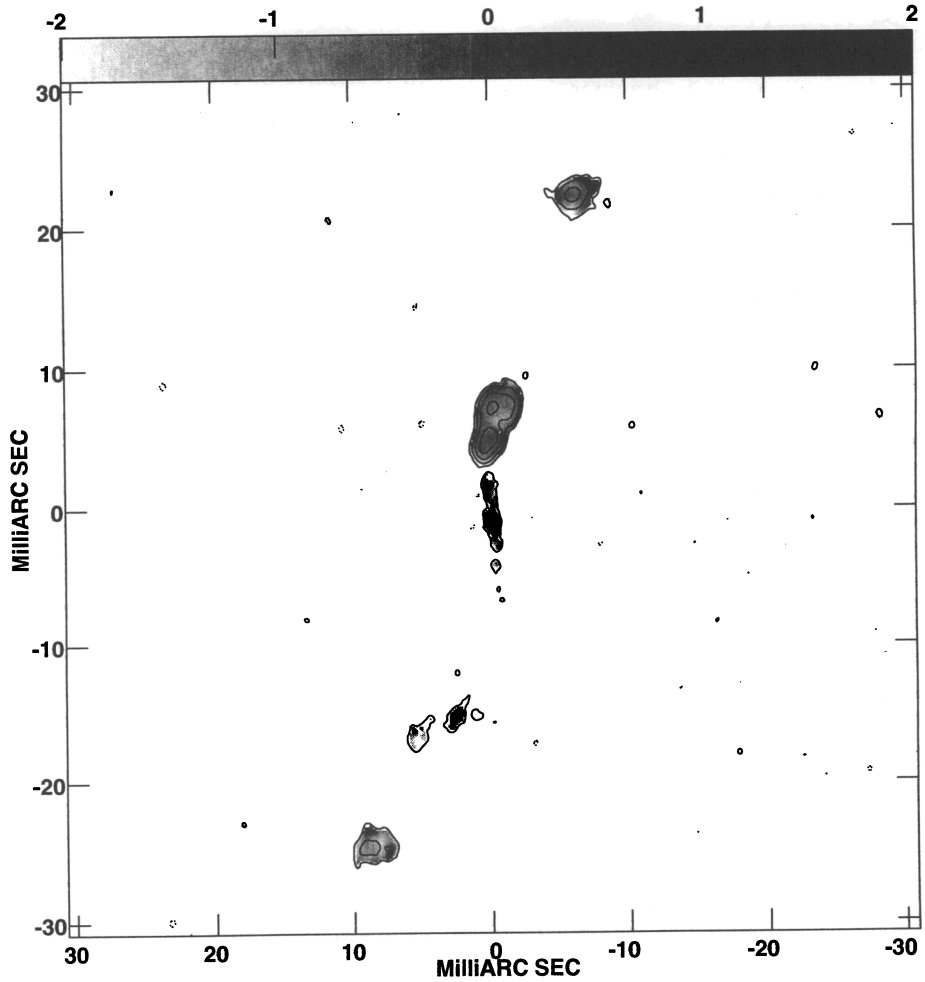

FIG. 6*b*

FIG. 6.—(*a*) The naturally weighted 15 GHz VLBI image of 2352+495. Contours are drawn at −0.75, 0.75, 1.5, 3, 6, ..., 96 mJy beam^{-1}. The synthesized beam is drawn in the lower left-hand corner and has dimensions 0.91 × 0.67 mas in position angle −3°. (*b*) A spectral index map made by combining our 15 GHz observations with the 8.4 GHz observations by Xu (1994) at the same resolution of 0.91 × 0.67 mas in position angle −3°. The gray-scale range is from −2 to 2. Contours are overlaid from the naturally weighted 15 GHz image at −0.75, 0.75, 3, 12, and 48 mJy beam^{-1}.

© American Astronomical Society • Provided by the NASA Astrophysics Data System

1996ApJ...463...95T

TABLE 7

CORE IDENTIFICATIONS IN THE PR CSOs

Source	Twin Lobes	Twin Jets	Twin Hot Spots	Steep Lobes	Inverted Core	Compact Core	Relative Motions	"S" Symmetry
0108+388.....	x	x	x	x	x	x	x	x
0404+768.....	x			x	x	x		
0710+439.....	x		x	x	x	x		x
1031+567.....	x		x	x				
1358+624.....	x			x	x	x		
2352+495.....	x	x	x	x	x	x	x	x

to be similarly enhanced. Furthermore, if these jets were strongly Doppler boosted by virtue of a favorable orientation close to the line of sight, then there should exist a much more numerous population of unbeamed sources that would have undetectable jets. This possibility was ruled out by Wilkinson et al. (1994). The second possibility is that the jet on one side has encountered a denser medium. This denser medium may cause entrainment and/or a greater emissivity of the radio plasma (Readhead et al. 1996a). Some evidence in support of asymmetries in the external medium is that the stronger hot spot is located on the more jetted side in three out of three sources in which hot spots can clearly be identified. And in 2352+495 the bright, broad, and complex B1-B2 jet feature has the appearance of a disrupted jet. A third possibility is that the jets possess an intrinsic asymmetry that causes one side to be brighter than the other.

We also find that three of these objects—0108+388, 0710+439, and 2352+495—all display a remarkable "S" symmetry about the center of activity. The same is true of another well-studied CSO, 1946+708 (Taylor et al. 1995). Thus four out of six confirmed CSOs from the PR and CJ survey display "S" symmetry. This may be explained by precession of the central engine. Precession has been invoked to explain the morphologies of several kiloparsec-scale radio sources (e.g., Hydra A [Taylor et al. 1990]; 3C 315, 3C 388, NGC 326 [Gower et al. 1982]). Begelman, Blandford, & Rees (1980) describe the precession resulting from two orbiting black holes. Readhead et al. (1996b) have applied this model to 2352+495 and found a wide range of black hole masses and separations that can feasibly produce precession periods of ~7000 yr.

5. CONCLUSIONS

We have located the center of activity in five out of six CSOs from the Pearson-Readhead (1988) sample. The core fraction tends to be low (<0.1) even at frequencies as high as 15 GHz. This low core fraction and the complex morphologies of CSOs have hindered the identification of the center of activity and even led to misidentifications in the past. We have shown that a reliable identification of the center of activity requires sensitive, multifrequency, multi-epoch VLBI observations. Further monitoring of all the CSOs reported on here would be useful to confirm our identifications of the centers of activity, and to obtain velocities for the jets and hot spots. In the future, phase-referenced observations of CSOs to nearby objects could be used to determine the absolute motions of the components in CSOs.

We thank the referee, Carla Fanti, for helpful comments on the manuscript. We are grateful to Wenge Xu for providing us with 8.4 GHz data from his Ph.D. thesis for the objects 0108+388, 0710+439, and 2352+495. This research has made use of the NASA/IPAC Extragalactic Database (NED), which is operated by the Jet Propulsion Laboratory, Caltech, under contract with NASA. This research has made use of data from the University of Michigan Radio Astronomy Observatory, which is supported by the NSF and by funds from the University of Michigan. This work was supported by the NSF under grants AST 91-17100 and AST 94-20018.

REFERENCES

Begelman, M. C., Blandford, R. D., & Rees, M. J. 1980, Nature, 287, 307
Conway, J. E., Myers, S. T., Pearson, T. J., Readhead, A. C. S., Unwin, S. C., & Xu, W. 1994, ApJ, 425, 568
Conway, J. E., Pearson, T. J., Readhead, A. C. S., Unwin, S. C., Xu, W., & Mutel, R. L. 1992, ApJ, 396, 62
Dallacasa, D., Fanti, C., Fanti, R., Schilizzi, R. T., & Spencer, R. E. 1995, A&A, 295, 27
de Kool, M., & Begelman, M. C. 1989, Nature, 338, 484
Fanaroff, B. L., & Riley, J. M. 1974, MNRAS, 167, 31P
Fanti, C., Fanti, R., Dallacasa, D., Schilizzi, R. T., Spencer, R. E., & Stanghellini, C. 1995, A&A, 302, 317
Gower, A. C., Gregory, P. C., Hutchings, J. B., & Unruh, W. G. 1982, ApJ, 262, 478
Henstock, D. R., Browne, I. W. A., Wilkinson, P. N., Taylor, G. B., Vermeulen, R. C., Pearson, T. J., & Readhead, A. C. S. 1995, ApJS, 100, 1
Lawrence, C. R., Zucker, J. R., Readhead, A. C. S., Unwin, S. C., Pearson, T. J., & Xu, W. 1996, ApJ, submitted
Padrielli, I., Iastman, W., Gregorini, L., Mantovani, F., & Spangler, S. 1991, A&A, 249, 351
Patnaik, A. R., Browne, I. W. A., Wilkinson, P. N., & Wrobel, J. M. 1992, MNRAS, 254, 655
Pearson, T. J., & Readhead, A. C. S. 1988, ApJ, 328, 114
Phillips, R. B., & Mutel, R. L. 1980, ApJ, 236, 89
———. 1982, A&A, 106, 21
Polatidis, A. G., Wilkinson, P. N., Xu, W., Readhead, A. C. S., Pearson, T. J., Taylor, G. B., & Vermeulen, R. C. 1995, ApJS, 98, 1
Readhead, A. C. S., Pearson, T. J., & Unwin, S. C. 1984, in IAU Symp. 110, VLBI and Compact Radio Sources, ed. R. Fanti, K. Kellerman, & G. Setti (Dordrecht: Reidel), 131
Readhead, A. C. S., Taylor, G. B., Pearson, T. J., & Wilkinson, P. N. 1996a, ApJ, 460, in press
Readhead, A. C. S., Taylor, G. B., Xu, W., Pearson, T. J., Wilkinson, P. N., & Polatidis, A. G. 1996b, ApJ, 460, 612
Schwab, F. R., & Cotton, W. D. 1983, AJ, 88, 688
Shepherd, M. C., Pearson, T. J., & Taylor, G. B. 1994, BAAS, 26, 987
———. 1995, BAAS, 27, 903
Taylor, G. B., Perley, R. A., Inoue, M., Kato, T., Tabara, H., & Aizu, K. 1990, ApJ, 360, 41
Taylor, G. B., Vermeulen, R. C., & Pearson, T. J. 1995, Proc. Natl. Acad. Sci., 92, 1138
Taylor, G. B., Vermeulen, R. C., Pearson, T. J., Readhead, A. C. S., Henstock, D. R., Browne, I. W. A., & Wilkinson, P. N. 1994, ApJS, 95, 345
Thakkar, D. D., Xu, W., Readhead, A. C. S., Pearson, T. J., Taylor, G. B., Vermeulen, R. C., Polatidis, A. G., & Wilkinson, P. N. 1995, ApJS, 98, 33
Wilkinson, P. N., Polatidis, A. G., Readhead, A. C. S., Xu, W., & Pearson, T. J. 1994, ApJ, 432, L87
Xu, W. 1994, Ph.D. thesis, California Inst. of Technology
Xu, W., Readhead, A. C. S., Pearson, T. J., Polatidis, A. G., & Wilkinson, P. N. 1995, ApJS, 99, 297

© American Astronomical Society • Provided by the NASA Astrophysics Data System